A Locking-free Kriging-based Timoshenko Beam Element with the Discrete Shear Gap Technique

Foek Tjong, WONG
Assistant Professor, Department of Civil Engineering
Petra Christian University, Surabaya, Indonesia
E-mail: wftjong@petra.ac.id

Adam, SULISTIO
Graduate Student, Department of Civil and Construction Engineering
National Taiwan University of Science and Technology, Taipei, Taiwan
E-mail: adamsulistio@gmail.com

ABSTRACT

The Kriging-based FEM (K-FEM) is an enhancement of the FEM through the use of Kriging interpolation in place of the conventional polynomial interpolation. The key advantage of the K-FEM is that the polynomial refinement can be performed without adding nodes or changing the element connectivity. In the development of the K-FEM for analyses of shear deformable beams, plates and shells, the well-known difficulty of shear locking also presents. This paper presents the K-FEM with the discrete shear gap (DSG) technique to eliminate the shear locking in the Timoshenko beam. The numerical tests show that the DSG technique can completely eliminate the shear locking for the Kriging-based beam element with cubic basis and three element-layer domain of influencing nodes. However, the DSG technique does not work well for the K-beam with linear (except with one element layer) and quadratic bases.

Keywords:

Timoshenko beam, Kriging-based finite element, shear locking, discrete shear gap

1. Introduction

An enhancement of the finite element method was proposed [1], in which the Kriging interpolation (KI) was utilized as the trial function in place of the conventional polynomial function. The KI in this proposed method was constructed for each element from a set of nodal values within a domain of influencing nodes (DOI) comprising the element itself and several layers of the surrounding elements. The DOI is thus a polygon in the 2D domain and a polyhedral in the 3D domain. The advantages of this novel proposed method are: (1) a high degree of polynomial function can be easily included in the trial function without adding any side or internal nodes in the element. (2) Highly accurate and smooth results for the state variables and their derivatives can be obtained even using the simplest form of elements. (3)

Furthermore, the computer implementation of the proposed method is very similar to that of the conventional FEM so that an existing general FEM code can be extended to include the method without a major change.

The proposed method [1] (hereafter referred to as Kriging-based finite element method, abbreviated to K-FEM) was subsequently improved through the use of adaptive correlation parameters and developed for analysis of Reissner-Mindlin plates and [2], [3]. A shortcoming of the K-FEM is that the trial function is discontinuous across the element boundaries, or in other words, it is nonconforming between interconnected elements. The issue of the nonconformity has been studied in [4] and it was found that the K-FEM with appropriate Kriging parameters always yields converging results.

In the development of the K-FEM for analyses of shear deformable beams, plates and shells, as in the FEM, the difficulty of shear locking also presents. In attempts to overcome this difficulty, the field-matching technique of Kanok-Nukulchai et al. [5], which works well in the element-free Galerkin method [6], has been tried on [7]. Using this technique, the shape functions for the rotational fileds were taken to be the derivatives of the shape functions for the defelction. It was found that the K-FEM with the field-macthing strategy yielded erroneous results. Accordingly, the field-matching technique is not applicable in the context of K-FEM. Another attempt was the introduction of assumed natural transverse shear strains in the K-FEM [8]. It was found that the assumed shear strain method can relieve the locking but it cannot eliminate the locking completely because the locations of shear-strain sampling points in the K-FEM cannot be determined exactly. Henceforth a sufficiently high degree basis function (cubic or higher) in the K-FEM for analyses of plates and shell structures was employed as a provisional solution to relieve the shear locking [2], [4], [7], [9]–[11]. The use of a high degree polynomial basis, however, cannot eliminate the locking completely and makes the computational cost high. Thus, an effective method to eliminate the shear locking in the K-FEM is indeed desirable.

In attempts to develop a locking free formulation for the K-FEM for analyses of plates and shells, it is instructive to study the K-FEM in the simpler problem of the Timoshenko beam in order to gain the understanding and insight about a locking-free device. In this spirit, Wong and Syamsoeyadi [12] recently developed the K-FEM for static and free vibration analyses of Timoshenko beams. In this development the shear locking was eliminated using the well-

known selective-reduced integration (SRI) technique. While the SRI technique can effectively eliminate the shear locking, the shear force resulting from this technique, however, is only accurate at the location of integration sampling point for shear force term, i.e. at the middle of the element. Moreover the SRI technique has been proved not applicable for the Kriging-based triangular plate bending element [7]. Therefore, a new shear locking elimination technique extendable to the Kriging-based Reissner-Mindlin plate element needs to be explored.

Bletzinger et al. (2000) [13] presented a unified approach to eliminate shear locking in shear deformable plates and shells, which is called the discrete shear gap (DSG) technique. In this approach, the shear gap is defined as the difference between the total deflection and the bending deflection, or in other words, it is the deflection corresponding to the shear strain. The shear gap is calculated at the element nodes (called the *discrete* shear gaps) and interpolated across the element domain. The substitute shear strain is then obtained from the derivatives of the interpolated discrete shear gaps. With this technique, a locking-free formulation of plate elements, either triangular or rectangular of any polynomial degree, can be carried out in a simple way. The technique was subsequently generalized to a more general concept applicable to other locking problems such as the membrane locking [14], [15].

The DSG technique has been applied not only in the conventional FEM, but also in recent alternative computational methods such as the edge-based smoothed FEM [16] and the node-based smoothed FEM [17]. The most recent application of the DSG approach is to combine the DSG three-node triangular element with the cell-based smoothed FEM to produce a three-node triangular plate element claimed to have some superior properties compared to many existing plate elements of the same class [18], [19]. These recent and somehow successful applications of the DSG technique suggest that it may also be effective to eliminate the shear locking in the Kriging-based shear deformable beams, plates and shells.

The aim of this paper is to present the development and testing of the K-FEM with the DSG technique to eliminate the shear locking in the context of Timoshenko beam model. The discretized equations were formulated using the standard displacement-based FE procedure on the variational form. The same Kriging shape functions ewre used for the deflection and rotation fields. The original displacement-based transverse shear strain was then replaced

with the DSG shear strain. A series of numerical tests were carried out to evaluate the effectiveness of the DGS technique to eliminate the shear locking. The results revealed that the Kriging-based Timoshenko beam (K-Beam-DSG) element with cubic basis and three element-layer DOI are free from shear locking, while the K-Beam-DSG with the other options, except with linear basis and one element layer, still suffers from shear locking.

2. Kriging Interpolation in the K-FEM

Named after Danie G. Krige, a South African mining engineer, Kriging is a well-known geostatistical technique for spatial data interpolation in geology and mining (see e.g. geostatistics literatures [20], [21]). The review on the KI in the framework of the K-FEM has been addressed in several previous published papers [3], [4], [12]. In this paper only the key points of the KI necessary for the subsequent development is addressed.

2.1. Kriging shape function

We consider a one-dimensional problem domain Ω where a continuous field variable (a scalar function) $u(x)$ is defined. The domain is represented by a set of properly scattered nodes x_I, I=1, 2, …, N, where N is the total number of nodes in the whole domain. Given N field values $u(x_1)$, …, $u(x_N)$, the problem of interest is to obtain an estimated value of u^{h} at a point $x \in \Omega$.

In the Kriging method, the unknown value $u^{\mathrm{h}}(x)$ is estimated from a linear combination of the field values at the neighboring nodes, i.e.

$$u^{\mathrm{h}}(x) = \sum_{i=1}^{n} \lambda_i u(x_i) \tag{1}$$

where λ_j's are the unknown *Kriging weights* and n is the number of nodes surrounding point x, inside and on the boundary of a subdomain $\Omega_{\mathbf{x}} \subseteq \Omega$, $n \le N$. Here small letters i and n are used instead of I and N to signify that the numbering is referred to the local (subdomain) numbering system.

In the context of the K-FEM [3], [4], [12], the nodes are identical to the finite element nodes, and the weights is identical to the shape functions. Furthermore, the subdomain $\Omega_{\mathbf{x}}$ in the K-FEM is composed of the element of interest and several layers of surrounding elements and referred to as the DOI. The number of element layers of the DOI can be one, two, or more. In the case of one layer, the DOI is the finite element itself and the K-FEM becomes identical to

the conventional FEM. Fig.1 illustrates a two-layer DOI encompassing local nodes 1, 2, 3 and 4.

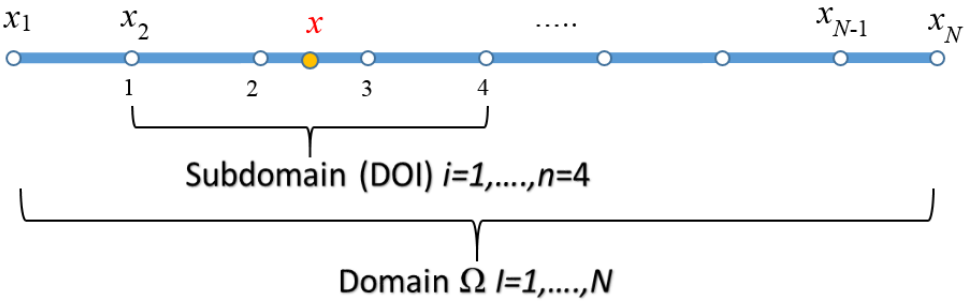

Fig 1. One-dimensional domain and a two element-layer subdomain

The Kriging weights λ_i, i=1,…,n, are obtained by solving the Kriging equation system:

$$\mathbf{R}\boldsymbol{\lambda} + \mathbf{P}\boldsymbol{\mu} = \mathbf{r}(x) \tag{2a}$$

$$\mathbf{P}^{\mathrm{T}}\boldsymbol{\lambda} = \mathbf{p}(x) \tag{2b}$$

in which

$$\mathbf{R} = \begin{bmatrix} C(h_{11}) & \ldots & C(h_{1n}) \\ \ldots & \ldots & \ldots \\ C(h_{n1}) & \ldots & C(h_{nn}) \end{bmatrix}; \quad \mathbf{P} = \begin{bmatrix} p_1(x_1) & \ldots & p_m(x_1) \\ \ldots & \ldots & \ldots \\ p_1(x_n) & \ldots & p_m(x_n) \end{bmatrix} \tag{2c}$$

$$\boldsymbol{\lambda} = \begin{bmatrix} \lambda_1 & \ldots & \lambda_n \end{bmatrix}^{\mathrm{T}}; \quad \boldsymbol{\mu} = \begin{bmatrix} \mu_1 & \ldots & \mu_m \end{bmatrix}^{\mathrm{T}} \tag{2d}$$

$$\mathbf{r}(x) = \begin{bmatrix} C(h_{1x}) & C(h_{2x}) & \ldots & C(h_{nx}) \end{bmatrix}^{\mathrm{T}}; \quad \mathbf{p}(x) = \begin{bmatrix} p_1(x) & \ldots & p_m(x) \end{bmatrix}^{\mathrm{T}} \tag{2e}$$

The entries in matrix **R**, $C(h_{ij})$, is the covariance between $U(x_i)$ and $U(x_j)$, which is a function of $h_{ij} = x_j - x_i$; i=1, … , n; j=1, … , n. Thus, **R** is the $n \times n$ matrix of covariance of $U(x)$ at nodes in the DOI, x_1, … , x_n. The capital '$U(x)$' here signifies the corresponding random process of the deterministic function $u(x)$. Matrix **P** is the $n \times m$ matrix of monomial values at the nodes, where m is the number of monomial terms. Vector $\boldsymbol{\lambda}$ is the unknown $n \times 1$ vector of Kriging weights and vector $\boldsymbol{\mu}$ is the unknown $m \times 1$ vector of Lagrange multipliers. On the right hand side of eqns. (2a) and (2b), vector $\mathbf{r}(x)$ is the $n \times 1$ vector of covariance between the nodes and the point of interest, x; and $\mathbf{p}(x)$ is the $m \times 1$ vector of monomial values at x. The entries in $\mathbf{r}(x)$, $C(h_{ix})$, is the covariance between $U(x_i)$ and $U(x)$, which is a function of $h_{ix} = x - x_i$. A necessary condition to make the Kriging equation system solvable

(nonsingular) is that the number of nodes in the DOI, *n*, should be equal or greater than the number monomial terms, *m*, i.e. $n \geq m$.

Solving the Kriging equation system, the vector of Kriging weights is given as

$$\boldsymbol{\lambda}^{\mathrm{T}} = \mathbf{p}^{\mathrm{T}}(x)\mathbf{A} + \mathbf{r}^{\mathrm{T}}(x)\mathbf{B} \tag{3a}$$

where

$$\mathbf{A} = (\mathbf{P}^{\mathrm{T}}\mathbf{R}^{-1}\mathbf{P})^{-1}\mathbf{P}^{\mathrm{T}}\mathbf{R}^{-1}\ , \quad \mathbf{B} = \mathbf{R}^{-1}(\mathbf{I} - \mathbf{P}\mathbf{A}) \tag{3b}$$

Here $\mathbf{A}$ is an $m \times n$ matrix, $\mathbf{B}$ is an $n \times n$ matrix, $\mathbf{I}$ is the $n \times n$ identity matrix.

The expression for the estimated value u^{h}, eqn. (1), can be restated in matrix form as

$$u^{\mathrm{h}}(x) = \boldsymbol{\lambda}^{\mathrm{T}}\mathbf{d} = \mathbf{N}(x)\mathbf{d} \tag{4}$$

where $\mathbf{d} = \left[u(x_1) \quad \ldots \quad u(x_n)\right]^{\mathrm{T}}$ is $n \times 1$ vector of nodal values and $\mathbf{N}(x) = \boldsymbol{\lambda}^{\mathrm{T}}$ is the matrix of Kriging shape functions. It is obvious that the Kriging weights are nothing but the shape functions.

2.2. Polynomial basis and correlation function

In order to construct Kriging shape functions, a polynomial basis function and a covariance function should be chosen. In the present research, as in the previous research on the K-FEM for analysis of Timoshenko beams [12], the polynomial bases of the degree one up to three are employed. The higher the polynomial degree, the more the element layers needed in the DOI because of the requirement $n \geq m$. The minimum number of DOI layers for different polynomial bases is listed in Table 1.

Table 1. Minimum number of layers for different polynomial basis

Polynomial basis	Monomial terms	*m*	Minimum number of layers
Linear	1 x	2	1
Quadratic	1 x x^2	3	2
Cubic	1 x x^2 x^3	4	3

A covariance $C(h)$ is more conveniently expressed in terms of correlation function, which is given as

$$\rho(h) = \frac{C(h)}{\sigma^2} \tag{5}$$

where h is the distance between points x and $x+h$ and σ^2 is the variance of the random function $U(x)$. The factor σ^2 has no effect on the resulting Kriging shape functions and it is taken equal to 1 in this study. There are many possibilities for the correlation function model in the area of geostatistics [20], [21], such as the Nugget-effect model, exponential model and spherical model. In the present study, as in the previous research [12], the Gaussian correlation function, i.e.

$$\rho(h) = \exp(-(\theta_r \frac{h}{d})^2) \tag{6}$$

and the quartic spline (QS), i.e.

$$\rho(h) = \begin{cases} 1-6(\theta_r \frac{h}{d})^2 + 8(\theta_r \frac{h}{d})^3 - 3(\theta_r \frac{h}{d})^4 & \text{for } 0 \le \theta_r \frac{h}{d} \le 1 \\ 0 & \text{for } \theta_r \frac{h}{d} > 1 \end{cases} \tag{7}$$

are chosen. In these equations, θ_r>0 is the correlation parameter and d is a scale factor to normalize the distance h. Factor d is taken to be the largest distance between any pair of nodes in the DOI.

The parameter θ_r is an important parameter affecting the validity of Kriging shape functions. Too small a value of θ_r deteriorates the partition of unity property of the shape functions [1], i.e.

$$\left| \sum_{i=1}^{n} N_i - 1 \right| \neq 1 \tag{8}$$

Conversely, too large a value of θ_r may make the Kriging equation system singular. Based on this facts, Plengkhom and Kanok-Nukulchai [1] proposed a rule of thumb for the lower and upper bounds of θ_r. Following this rule, the value of θ_r should be selected so that it satisfies the lower bound criterion,

$$\left| \sum_{i=1}^{n} N_i - 1 \right| \le 1 \times 10^{-10+a} \tag{9}$$

where a is the degree of basis function, and the upper bound criterion,

$$\det(\mathbf{R}) \le 1 \times 10^{-b} \tag{10}$$

where b is the dimension of the problem. For the 1D problem and quadratic basis function, for example, a=2 and b=1.

The range of appropriate values of θ_r varies with the number of monomial terms m, the number of the nodes in the DOI, n, and the correlation model used [1], [2]. In other words, it

depends on the polynomial basis, the number of element layers, and type of the correlation function employed in an analysis. The range of θ_r for 1D problems satisfying the lower and upper bound criteria, eqns. (9) and (10), have been numerically examined [12] and the results are presented in Table 2. It is recommended to take the mid-value between the upper and lower bounds to ensure the good quality of KI.

Table 2. The lower and upper bounds of θ_r for 1D problems

Polynomial basis	Number of layers	Gaussian $\rho(h)$		Quartic spline $\rho(h)$	
		Lower bound	Upper bound	Lower bound	Upper bound
Linear	1	0	0.2295	0	0.098
	2	10^{-4}	1.0	10^{-5}	0.44
	3	10^{-4}	1.9	10^{-5}	0.86
Quadratic	2	10^{-4}	1.0	10^{-5}	0.44
	3	10^{-4}	1.9	10^{-6}	0.86
Cubic	3	10^{-4}	1.9	10^{-8}	0.86

3. Formulation of Kriging-based Timoshenko Beam Element

We consider a beam of length L with the cross sectional area and moment of inertia A and I, respectively. The beam is made from a homogeneous and isotropic material with the modulus of elasticity E, shear modulus G, and mass density ρ (per unit volume). A Cartesian coordinate system (x,y,z) is established where the x-axis coincides with the neutral axis and y- and z-axes coincide with the principal axes of the cross section (Fig. 2). The beam is subjected to dynamic distributed transversal load $q=q(x, t)$, distributed moment $m=m(x, t)$, and axial tensile force $P=P(t)$, $0 \le x \le L$, $t \ge 0$. In the Timoshenko beam theory, the motion of the beam due to the external loads is described using two independent field variables, namely the transverse displacement (deflection) of the neutral axis $w=w(x,t)$ and the rotation of the cross-section $\theta= \theta(x,t)$. The sign convention for these variables is shown in Fig. 2.

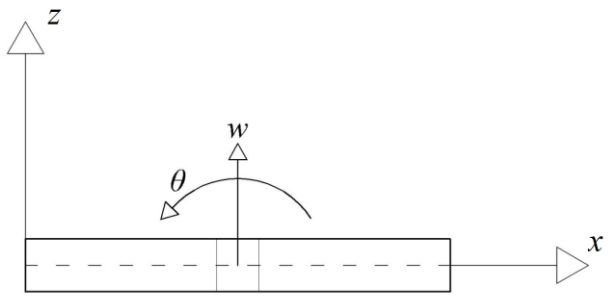

Fig 2. Coordinate system and positive directions for the deflection and rotation

The governing equation for the motion of the beam at time t, including the axial load effect, can be expressed in a variational form as

$$\begin{aligned}&\int_0^L \delta w\, \rho A \ddot{w}\, dx + \int_0^L \delta\theta\, \rho I\, \ddot{\theta}\, dx \\ &+ \int_0^L \delta\theta_{,x}\, EI\theta_{,x}\, dx + \int_0^L \delta\gamma\, GA_s\, \gamma\, dx + \int_0^L \delta w_{,x}\, P\, w_{,x}\, dx \\ &= \int_0^L \delta w\, q\, dx + \int_0^L \delta\theta\, m\, dx\end{aligned} \tag{11}$$

In this equation,

$$\gamma = w_{,x} - \theta \tag{12}$$

is the transverse shear strain, and $A_s=kA$ is the effective shear area, where k is a shear correction factor that is dependent upon the cross-section geometry. The double dots signify the second partial derivative of the corresponding variable with respect to the time variable t, whereas the comma signifies the first partial derivative of with respect to the variable next to it (i.e. x). The operator δ signifies the variational operation on the corresponding variable. A detail derivation of the variational equation, eqn. (11), using the Hamilton's principle is given in references [22], [23].

The bending moment and shear force along the beam can be calculated from the deflection w and rotation θ as follows:

$$M = EI\ \theta_{,x} \tag{13}$$

$$Q = GA_s\ \left(w_{,x} - \theta\right) + P\, w_{,x} \tag{14}$$

To obtain an approximate solution using the concept of KI with layered-element DOI, let the beam is subdivided into N_{el} elements and N nodes. We then consider an element with its DOI that contains n nodes, as illustrated in Fig. 3. The field variables w and θ over the element are approximated using KI as follows

$$w = \mathbf{N}_w(x)\ \mathbf{d}(t) \tag{15a}$$

$$\theta = \mathbf{N}_\theta(x)\ \mathbf{d}(t) \tag{15b}$$

where

$$\mathbf{N}_w(x) = [N_1(x) \quad 0 \quad N_2(x) \quad 0 \quad \cdots \quad N_n(x) \quad 0] \tag{15c}$$

$$\mathbf{N}_\theta(x) = [0 \quad N_1(x) \quad 0 \quad N_2(x) \quad \cdots \quad 0 \quad N_n(x)] \tag{15d}$$

are the matrix of Kriging shape functions for the deflection and rotation, respectively, and

$$\mathbf{d}(t) = \begin{bmatrix} w_1(t) & \theta_1(t) & w_2(t) & \theta_2(t) & \cdots & w_n(t) & \theta_n(t) \end{bmatrix}^{\mathrm{T}} \tag{15e}$$

is the vector of nodal displacement. Variable x here refer to the local (element) coordinate system. The number of nodes, n, depends on the number of elements used in the DOI and is different for the interior and exterior elements. For example, for the element with two-layer DOI, n=4 for the exterior element and n=3 for the interior element.

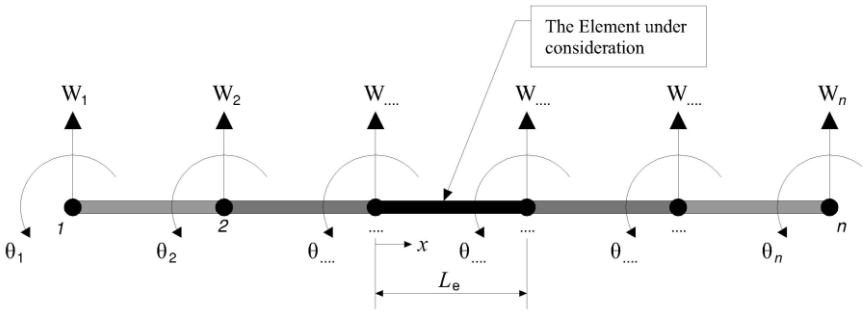

Fig 3. A typical beam element and its domain of influencing nodes (DOI)

Substituting eqns. (15a) and (15b) into eqn. (11) and carrying out the standard finite element formulation yield the discretized system of equations

$$\mathbf{m}\ddot{\mathbf{d}}(t) + (\mathbf{k} + P\,\mathbf{k}_{\mathrm{g}})\mathbf{d}(t) = \mathbf{f}(t) \tag{16}$$

In this equation,

$$\mathbf{m} = \int_0^{L_{\mathrm{e}}} \mathbf{N}_w^{\mathrm{T}}\, \rho A \mathbf{N}_w\, dx + \int_0^{L_{\mathrm{e}}} \mathbf{N}_\theta^{\mathrm{T}}\, \rho I\, \mathbf{N}_\theta\, dx \tag{17}$$

is the element consistent mass matrix,

$$\mathbf{k} = \int_0^{L_{\mathrm{e}}} \mathbf{B}_\theta^{\mathrm{T}}\, EI\, \mathbf{B}_\theta\, dx + \int_0^{L_{\mathrm{e}}} \mathbf{B}_\gamma^{\mathrm{T}}\, GA_{\mathrm{s}}\, \mathbf{B}_\gamma\, dx \tag{18}$$

is the element stiffness matrix,

$$\mathbf{k}_{\mathrm{g}} = \int_0^{L_{\mathrm{e}}} \mathbf{B}_w^{\mathrm{T}} \mathbf{B}_w\, dx \tag{19}$$

is the element geometrical stiffness matrix, and

$$\mathbf{f}(t) = \int_0^{L_{\mathrm{e}}} \mathbf{N}_w^{\mathrm{T}}\, q\, dx + \int_0^{L_{\mathrm{e}}} \mathbf{N}_\theta^{\mathrm{T}}\, m\, dx \tag{20}$$

is the element equivalent nodal force vector. The order of all square matrices and vectors are $2n$. In eqns. (18) and (19), matrices $\mathbf{B}_\theta$, $\mathbf{B}_w$ and $\mathbf{B}_\gamma$ are defined as follows:

$$\mathbf{B}_\theta = \frac{d}{dx}\mathbf{N}_\theta, \quad \mathbf{B}_w = \frac{d}{dx}\mathbf{N}_w \tag{21a}$$

$$\mathbf{B}_\gamma = \mathbf{B}_w - \mathbf{N}_\theta \tag{21b}$$

The unknowns of eqn. (16) are the element nodal acceleration vector $\ddot{\mathbf{d}}(t)$ and the nodal displacement vector $\mathbf{d}(t)$.

The discretized equations for static, free vibration, and buckling problems can be obtained from eqn. (16) by simply reducing it to

$$\mathbf{kd} = \mathbf{f} \tag{22}$$

$$\mathbf{m}\ddot{\mathbf{d}}(t) + \mathbf{kd}(t) = \mathbf{0} \tag{23}$$

$$(\mathbf{k} + P\mathbf{k}_{\mathrm{g}})\mathbf{d} = \mathbf{0} \tag{24}$$

respectively.

The corresponding global discretized equations of these equations can be obtained using the finite element assembly procedure. It should be mentioned here that the assembly process involves all nodes in the DOI, not only the element nodes as in the conventional FEM.

4. Application of the Discrete Shear Gap Concept

It is well known in the FEM that the pure displacement-based formulation of Timoshenko beam (with exact integration of all integral) leads to the shear locking phenomenon [24]–[29]. The same is true for the Kriging-based Timoshenko beam element [12], even for the element with cubic polynomial basis function. The primary cause of this locking is the inability of the approximate shear strain to vanish as the beam length-to-thickness ratio becomes large. The basic idea of the discrete shear gap (DSG) concept [13], [14] is to replace the troublesome kinematic shear strain with a substitute shear strain field determined from the derivative of interpolated discrete shear gaps. This section presents a review of the DSC concept and its application to Timoshenko beam elements with the KI.

To apply the DSG concept, we begin with the definition of *shear gap*, i.e.

$$\Delta w_\gamma(x) = \int_{x_0}^{x} \gamma \, dx \tag{25}$$

where $\Delta w_\gamma(x)$ is the shear gap at point x, and x_0 is the position of a chosen reference point. Inserting eqn. (12) into this equation results in

$$\Delta w_\gamma(x) = w\big|_{x_0}^{x} - \int_{x_0}^{x} \theta\, dx \tag{26a}$$

$$\Delta w_\gamma(x) = (w(x) - w(x_0)) - \int_{x_0}^{x} \theta\, dx = \Delta w\ (x) - \Delta w_{\mathrm{b}}(x) \tag{26b}$$

In these equations, Δw is the increase of the actual deflection between the positions x and x_0, and Δw_b is the increase of the deflection due to bending action. The shear gap $\Delta w_\gamma(x)$ thus represents the increase of the deflection due to shearing action.

The *discrete* shear gap at a finite element node with position x_i, $\Delta w_{\gamma i}$, is defined as

$$\Delta w_{\gamma i} = \Delta w_\gamma(x_i) = w\big|_{x_0}^{x_i} - \int_{x_0}^{x_i} \theta\, dx \tag{27}$$

A modified shear gap field is defined as the interpolation of the nodal shear gaps, i.e.

$$\Delta \bar{w}_\gamma(x) = \sum_{i=1}^{n} N_i(x)\ \Delta w_{\gamma i} \tag{28}$$

In the framework of the standard FEM, n is the number of number of nodes in the element and $N_i(x)$, i=1, ..., n are the shape functions. In the present research, however, n is the number of nodes in the DOI and $N_i(x)$ are Kriging shape functions. Differentiating eqn. (28) gives the *substitute* shear strain, i.e.

$$\bar{\gamma}(x) = \sum_{i=1}^{n} N_{i,x}\, \Delta w_{\gamma i} = \bar{\mathbf{B}}_{\gamma 1} \mathbf{w}_\gamma \tag{29a}$$

where

$$\bar{\mathbf{B}}_{\gamma 1} = \begin{bmatrix} N_{1,x} & N_{2,x} & \cdots & N_{n,x} \end{bmatrix} \tag{29b}$$

$$\mathbf{w}_\gamma = \begin{bmatrix} \Delta w_{\gamma 1} & \Delta w_{\gamma 2} & \cdots & \Delta w_{\gamma n} \end{bmatrix}^{\mathrm{T}} \tag{29c}$$

To avoid the shear locking problem, the kinematic shear strain γ, eqn. (12), is replaced with $\bar{\gamma}$, eqn. (29a). In order to implement this technique to the Kriging-based beam elements, we first need to express the nodal shear gaps in the DOI, $\mathbf{w}_\gamma$, in terms of the degrees of freedom of the Timoshenko beam. Choosing node 1 to be the reference point (see Fig. 3) and inserting eqn. (15b) into eqn. (27), the discrete shear gaps is given as

$$\Delta w_{\gamma i} = w_i - w_1 - \left(\int_{x_1}^{x_i} \mathbf{N}_\theta(x)\, dx\right)\mathbf{d} \tag{30}$$

Evaluating the discrete shear gaps for nodes 1 to n and writing them in a matrix form, the discrete shear gaps for all nodes in the DOI can be expressed as

$$\mathbf{w}_\gamma = \bar{\mathbf{B}}_{\gamma 2}\mathbf{d} \tag{31a}$$

where

$$\bar{\mathbf{B}}_{\gamma 2} = \begin{bmatrix} 0 & 0 & 0 & 0 & 0 & 0 & \cdots & 0 & 0 \\ -1 & -\int_{x_1}^{x_2} N_1 dx & 1 & -\int_{x_1}^{x_2} N_2 dx & 0 & -\int_{x_1}^{x_2} N_3 dx & \cdots & 0 & -\int_{x_1}^{x_2} N_n dx \\ -1 & -\int_{x_1}^{x_3} N_1 dx & 0 & -\int_{x_1}^{x_3} N_2 dx & 1 & -\int_{x_1}^{x_3} N_3 dx & \cdots & 0 & -\int_{x_1}^{x_3} N_n dx \\ \vdots & \vdots & \vdots & \vdots & \vdots & \vdots & \vdots & \vdots & \vdots \\ -1 & -\int_{x_1}^{x_n} N_1 dx & 0 & -\int_{x_1}^{x_n} N_2 dx & 0 & -\int_{x_1}^{x_n} N_3 dx & \cdots & 1 & -\int_{x_1}^{x_n} N_n dx \end{bmatrix} \tag{31b}$$

Substituting eqn. (31a) into eqn. (29a) yields

$$\bar{\gamma}(x) = \bar{\mathbf{B}}_{\gamma 1}\bar{\mathbf{B}}_{\gamma 2}\mathbf{d} = \bar{\mathbf{B}}_{\gamma}\mathbf{d} \tag{32}$$

The implementation of the DSG concept is accomplished by replacing matrix $\mathbf{B}_\gamma$ in the expression for the element stiffness matrix, eqn. (18), with matrix $\bar{\mathbf{B}}_\gamma$ as defined in eqn. (32).

5. Numerical Results

The performance of the K-Beam-DSG elements were evaluated using the pure bending and clamped-clamped beam. The shear correction factor used was given as ([30], cited in [22], [23])

$$k = \frac{10(1+\nu)}{12+11\nu} \tag{33}$$

Special attention given to evaluate the effectiveness of the DSG technique in eliminating the shear locking. The K-FEM options used comprised linear up to cubic basis functions, one to three element layers, and the Gaussian or QS correlation functions with the mid-value correlation parameters between the lower and upper bound values (Table 2). Abbreviations of the form P*-*-G or P*-*-QS were used to denote different K-FEM options. The first asterisk represents the polynomial basis, while the second represents the number of DOI element layers. The last letter(s) represent the Gaussian (G) or quartic spline (QS) correlation function. For example, abbreviation P2-3-QS means the K-FEM options of quadratic basis function, three element layers, and quartic spline correlation function (with mid-value correlation parameter).

In all calculations, three Gaussian sampling points were used to evaluate the integrations in the element stiffness matrix equations, eqn. (18), while two sampling points were used to

evaluate the integration in the element consistent nodal load vector, eqn. (20) and $\bar{\mathbf{B}}_{\gamma 2}$ (31b). The abovementioned number of sampling points were chosen because we found by trial-and-error that they can provide accurate results with minimum effort.

5.1. Pure bending test

A cantilever beam of rectangular cross-section $b \times h$ subjected to an end moment was modelled with meshes of regular and irregular node distributions as shown in Fig. 4. The beam is in pure bending state with constant bending moment, M, and zero shear force along the beam. This problem may be regarded as a constant curvature patch test for beam finite elements. An element is said to pass the test if it can reproduce the exact deflection, rotation, bending moment, and shear forces for any mesh.

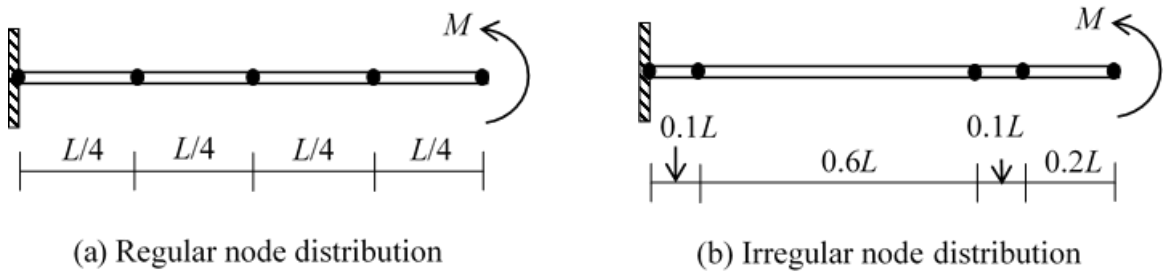

Fig 4. Cantilever beam modelled with (a) regular and (b) irregular node distributions

The beam was analyzed using the K-Beam-DSG with different polynomial bases, number of layers, and correlation functions. Numerical values used in the analyses were L=10 m, b=2 m, E=2000 kN/m^2, ν=0.3 and M=1 kN-m. Two different length-to-thickness ratios were considered. One was moderately thick, i.e. L/h=5, and the other was extremely thin, i.e. L/h=10000. The resulting deflections and rotations at the free end, w_L and θ_L, were observed and then normalized to the corresponding exact solutions, i.e.

$$w_{L\text{exact}} = \frac{ML^2}{2EI}, \quad \theta_{L\text{exact}} = \frac{ML}{EI} \tag{34}$$

The resulting bending moments and shear forces at the clamped end, calculated using eqns. (13) and (14), were observed as well. The bending moments were then normalized to the exact bending moment, M. The shear forces, however, were not normalized because of the zero exact shear force.

The results showed that the K-Beam-DSG produced values of the deflection, rotation and bending moment with at least seven digit accuracy (nearly exact values) both for the thick and thin beams with the regular node distribution. The maximum error for the shear force, however, was in the order of 10^{-5} (for the case of the thin beam analyzed using the P1-3-G option). Very accurate results for the deflection, rotation, and bending moment of the thick and thin beams were also obtained for the case of the irregular node distribution, with the accuracy at least 5 digits (for the thin beam analyzed using the P1-3-G option). Table 3 presents the results for the thin beam modelled with the irregular node distribution (the most critical case). It was seen that for this case the accuracy of the shear force (the maximum error is in the order of 10^{-2}) was lower compare to the thin beam modelled with regular node distribution. It is worthy to mention here that the standard finite element and Kriging-based Timoshenko beam elements with the selective reduce integration are unable to produce correct values for the shear force computed using eqn. (14) [12], [29].

Overall, the results indicate that the K-Beam-DSG with different analysis options practically pass the constant curvature patch test. The K-Beam-DSG elements with the Gaussian correlation function in general produce less accurate results than those with the QS. In this simple problem there is no indication of shear locking.

Table 3. Analysis results using various K-Beam-DSG options

K-Beam-DSG options	$w_L / w_{L\,\text{exact}}$	$\theta_L / \theta_{L\,\text{exact}}$	$M_0 / M_{0\,\text{exact}}$	V_0
P1-1-QS	1.0000000	1.0000000	0.9999999	-5.36E-09
P1-2-QS	0.9999997	0.9999997	0.9999997	4.93E-05
P1-3-QS	1.0000000	1.0000000	1.0000000	-2.02E-05
P2-2-QS	1.0000000	1.0000001	1.0000000	-9.21E-07
P2-3-QS	0.9999999	0.9999999	0.9999998	3.41E-06
P3-3-QS	1.0000001	1.0000001	1.0000002	-1.12E-07
P1-1-G	1.0000000	1.0000000	0.9999999	-8.61E-09
P1-2-G	1.0000000	0.9999998	1.0000004	2.64E-03
P1-3-G	1.0000056	1.0000006	1.0000367	-6.28E-02
P2-2-G	0.9999999	0.9999999	0.9999999	2.71E-03
P2-3-G	0.9999991	0.9999994	0.9999990	-9.55E-03
P3-3-G	1.0000002	1.0000001	1.0000005	9.21E-03

5.2. Investigation on shear locking

To investigate the effectiveness of the DSG technique in eliminating the shear locking, we considered the clamped-clamped beam with the finite element model as shown in Fig. 5. The height of the beam was varied from moderately thick, L/h=5, up to extremely thin, L/h=10^4. The geometrical and material properties of the beam were the same as in the pure bending test (Sec. 2.1.1) with the distributed load q=1 kN/m. The beam was analyzed using the K-Beam-DSG elements with different K-FEM options. The resulting deflections of the beam mid-span were observed and normalized to the exact solution, i.e.

$$w_{\text{exact}} = \frac{qL^4}{384EI} + \frac{qL^2}{8GA_s} \tag{35}$$

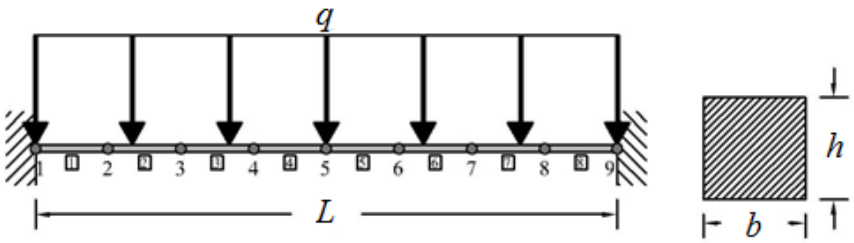

Fig 5. Clamped-clamped beam modelled with mesh of eight elements

The results were presented in Table 4. The results obtained from the use of K-Beam-DSG with the QS correlation function were reported here. The corresponding results for the Gaussian correlation function had similar locking behavior.

Table 4. Normalized deflections of the beam mid-span using various K-Beam-DSG options

K-Beam-DSG options	L/h=5	L/h=10	L/h=100	L/h=1000	L/h=10000
P1-1-QS	0.958	0.944	0.938	0.938	0.938
P1-2-QS	0.979	1.000	0.959	0.206	0.003
P1-3-QS	0.983	0.996	0.983	0.517	0.012
P2-2-QS	0.994	1.001	0.993	0.540	0.011
P2-3-QS	0.991	1.003	0.994	0.505	0.010
P3-3-QS	0.999	1.001	1.001	1.001	1.001

It is seen from Table 4 that for moderately thick to thin beams (i.e. L/h=5 to 100), all K-Beam-DSG options could produce accurate results. However, when the beam becomes thinner, it is apparent that only the K-Beam–DSGs with P1-1-QS and P3-3-QS options show no locking. Further testing of the P1-1-QS and P3-3-QS options with the values of L/h

greater than 10^4 reveals that there is no locking up to $L/h=10^7$. For L/h over 10^7 the results become inaccurate because of the stiffness matrix ill condition. It is worthy to note that the K-Beam-DSG P1-1-QS is actually identical to the locking-free linear Timoshenko beam element with the DSG presented in [13], [14].

To investigate further why the shear locking phenomenon still occurs on the K-Beam-DSGs with linear (except with one layer) and quadratic basis functions, we considered the shear forces calculated using the 'successful' options, i.e. P1-1-QS and P3-3-QS, and 'unsuccessful' options, i.e. P1-3-QS and P2-3-QS, for the extremely thin beam ($L/h=10^4$). The shear force diagrams were shown in Figs. 6a and 6b, respectively. Fig. 6a shows that the shear force distributions obtained from the K-Beam-DSGs with P1-1-QS and P3-3-QS options oscillate about the exact shear force distribution. These oscillations, however, are relatively very mild compared to the violent shear force oscillations obtained from the K-Beam-DSGs with P1-3-QS and P2-3-QS (Fig. 6b). Furthermore, the total area under the shear force curves of the P1-1-QS and P3-3-QS seems equal to the total area under the exact curve. That is the reason why the K-Beam-DSGs with P1-1-QS and P3-3-QS are locking free while the K-Beam-DSGs with the other options are not locking free.

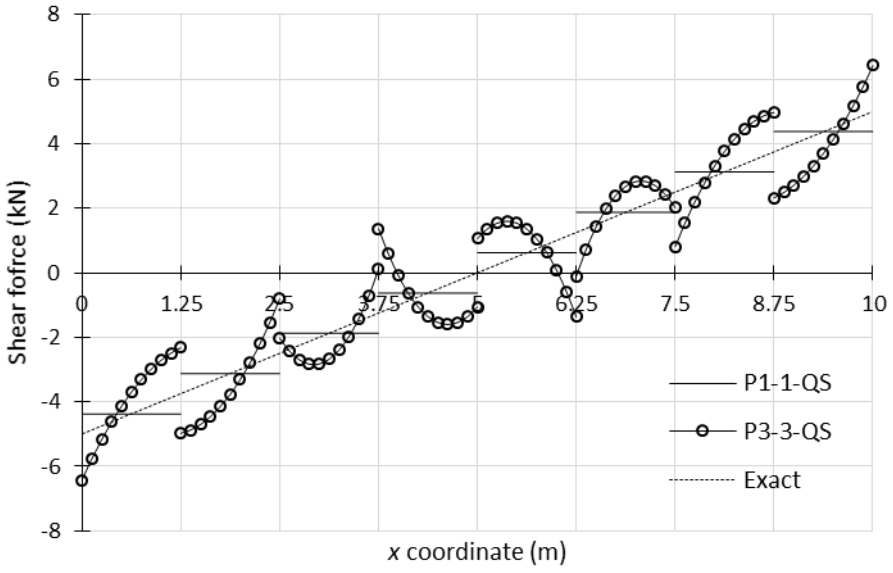

Fig 6a. Shear force diagram obtained using K-Beam-DSG with options P1-1-QS and P3-3-QS

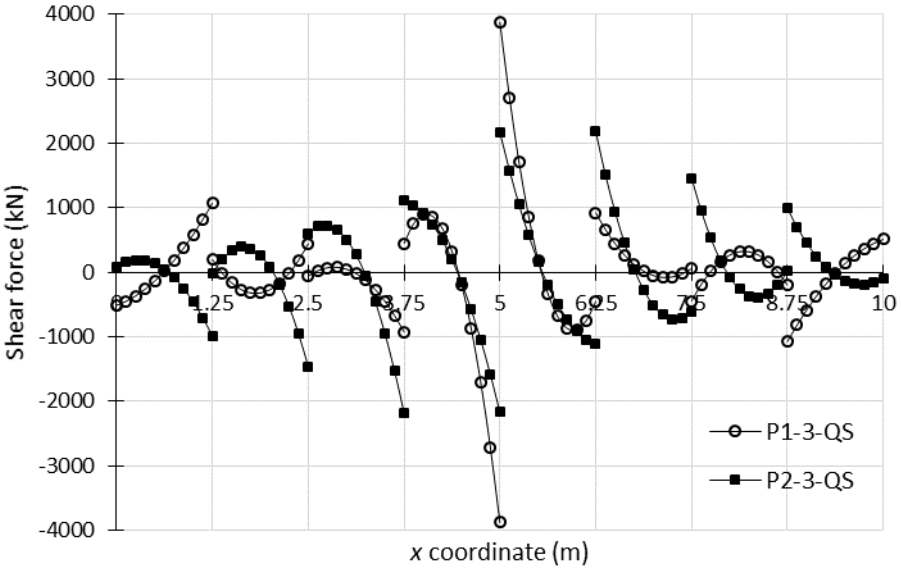

Fig 6b. Shear force diagram obtained using K-Beam-DSG with options P1-3-QS and P2-3-QS

6. Conclusions

Kriging-based Timoshenko beam elements with DSG have been developed and tested. The results showed that the DSG method was effective to eliminate the shear locking for the element with cubic basis function and three element-layer DOI while for the other K-FEM options was not so effective. The resulting shear force distributions were not very accurate for thin beams with small number of elements. The application of the DSG technique in the Timoshenko beam model provides understanding and insight to extend the application to the Kriging-based Reissner-Mindlin plate model, which is now still ongoing research.

Acknowledgements

We gratefully acknowledge that this research has been partly supported by the internal research funding of Petra Christian University, Indonesia.

References

[1] K. Plengkhom and W. Kanok-Nukulchai, "An Enhancement of Finite Element Method with Moving Kriging Shape Functions," *Int. J. Comput. Methods*, vol. 02, no. 04, pp. 451–475, Dec. 2005.

[2] F. T. Wong and W. Kanok-Nukulchai, "Kriging-based Finite Element Method for Analyses of Reissner-Mindlin plates," in *Proceedings of the Tenth East-Asia Pacific Conference on Structural Engineering and Construction, Emerging Trends: Keynote*

Lectures and Symposia, 2006, pp. 509–514.

[3] F. T. Wong and W. Kanok-Nukulchai, "Kriging-Based Finite Element Method : Element-By-Element Kriging Interpolation," *Civ. Eng. Dimens.*, vol. 11, no. 1, pp. 15–22, 2009.

[4] F. T. Wong and W. Kanok-Nukulchai, "On the Convergence of the Kriging-based Finite Element Method," *Int. J. Comput. Methods*, vol. 06, no. 01, pp. 93–118, Mar. 2009.

[5] W. Kanok-Nukulchai, W. Barry, K. Saran-Yasoontorn, and P. H. Bouillard, "On Elimination of Shear Locking in the Element-free Galerkin Method," *Int. J. Numer. Methods Eng.*, vol. 52, no. 7, pp. 705–725, Nov. 2001.

[6] T. Belytschko, Y. Y. Lu, and L. Gu, "Element-free Galerkin Methods," *Int. J. Numer. Methods Eng.*, vol. 37, no. 2, pp. 229–256, Jan. 1994.

[7] F. T. Wong, "Kriging-based Finite Element Method for Analyses of Plates and Shells," Asian Institute of Technology, Pathumthani, 2009.

[8] F. T. Wong and W. Kanok-Nukulchai, "On Alleviation of Shear Locking in the Kriging-Based Finite Element Method," in *Proceedings of International Civil Engineering Conference "Towards Sustainable Engineering Practice,"* 2006, pp. 39–47.

[9] F. T. Wong, "Kriging-Based Finite Element Methods for Analyses of Shear Deformable Beams and Plates," in *Proceedings of the 6th Civil Engineering Conference in Asian Region and Annual HAKI Conference*, 2013, p. Paper ID#63.

[10] F. T. Wong and W. Kanok-Nukulchai, "A Kriging-based Finite Element Method for Analyses of Shell Structures," in *Proceedings of the Eighth World Congress on Computational Mechanics and the Fifth European Congress on Computational Methods in Applied Sciences and Engineering*, 2008, no. ECCOMAS, p. a1247.

[11] F. T. Wong, Y. Christabel, P. Pudjisuryadi, and W. Kanok-Nukulchai, "Testing of the Kriging-based Finite Element to Shell Structures with Varying Thickness," *Procedia Eng.*, vol. 125, pp. 843–849, 2015.

[12] F. T. Wong and H. Syamsoeyadi, "Kriging-based Timoshenko Beam Element for Static and Free Vibration Analyses," *Civ. Eng. Dimens.*, vol. 13, no. 1, pp. 42–49, 2011.

[13] K.-U. Bletzinger, M. Bischoff, and E. Ramm, "A unified approach for shear-locking-free triangular and rectangular shell finite elements," *Comput. Struct.*, vol. 75, no. 3, pp. 321–334, Apr. 2000.

[14] M. Bischoff, F. Koschnick, and K. Bletzinger, "Stabilized DSG Elements – A New Paradigm in Finite Element Technology," *Proc. 4th Eur. LS-DYNA Users Conf.*, no. 0, 2003.

[15] F. Koschnick, M. Bischoff, N. Camprubí, and K. U. Bletzinger, "The discrete strain gap method and membrane locking," *Comput. Methods Appl. Mech. Eng.*, vol. 194, pp. 2444–2463, 2005.

[16] H. Nguyen-Xuan, G. R. Liu, C. Thai-Hoang, and T. Nguyen-Thoi, "An edge-based smoothed finite element method (ES-FEM) with stabilized discrete shear gap technique for analysis of Reissner–Mindlin plates," *Comput. Methods Appl. Mech. Eng.*, vol. 199, no. 9–12, pp. 471–489, Jan. 2010.

[17] H. Nguyen-Xuan, T. Rabczuk, N. Nguyen-Thanh, T. Nguyen-Thoi, and S. Bordas, "A node-based smoothed finite element method with stabilized discrete shear gap technique for analysis of Reissner–Mindlin plates," *Comput. Mech.*, vol. 46, no. 5, pp. 679–701, 2010.

[18] T. Nguyen-Thoi, M. H. Nguyen-Thoi, T. Vo-Duy, and N. Nguyen-Minh, "Development of the Cell-based Smoothed Discrete Shear Gap Plate Element (CS-FEM-DSG3) using Three-Node Triangles," *Int. J. Comput. Methods*, no. January 2016, p. 1540015, 2015.

[19] T. Nguyen-Thoi, P. Phung-Van, H. Nguyen-Xuan, and C. Thai-Hoang, "A cell-based smoothed discrete shear gap method using triangular elements for static and free vibration analyses of Reissner-Mindlin plates," *Int. J. Numer. Methods Eng.*, vol. 91, no. 7, pp. 705–741, Aug. 2012.

[20] R. A. Olea, *Geostatistics for Engineers and Earth Scientistics*. Boston: Kluwer Academic Publishers, 1999.

[21] H. Wackernagel, *Multivariate Geostatistics*, 3rd ed. Berlin: Springer, 2003.

[22] Z. Friedman and J. B. Kosmatka, "An Improved Two-node Timoshenko Beam Finite Element," *Comput. Struct.*, vol. 47, no. 3, pp. 473–481, May 1993.

[23] J. B. Kosmatka, "An improved two-node finite element for stability and natural frequencies of axial-loaded Timoshenko beams," *Comput. Struct.*, vol. 57, no. 1, pp. 141–149, Oct. 1995.

[24] R. D. Cook, D. S. Malkus, M. E. Plesha, and R. J. Witt, *Concepts and Applications of Finite Element Analysis*, 4th ed. John Wiley & Sons, Ltd, 2002.

[25] K. J. Bathe, *Finite Element Procedures*. New Jersey: Prentice-Hall, 1996.

[26] T. J. R. Hughes, *The Finite Element Method: Linear Static and Dynamic Finite Element Analysis*. New Jersey: Prentice-Hall, 1987.

[27] J. N. Reddy, *An Introduction to the Finite Element Method (Engineering Series)*. Singapore: McGraw-Hill Science/Engineering/Math, 2006.

[28] G. Prathap, "Finite Element Analysis as Computation," 2001. [Online]. Available: http://www.cmmacs.ernet.in/cmmacs/online_contents.html. [Accessed: 05-Feb-2016].

[29] G. Prathap, "The Finite Element Method in Structural Mechanics," *Springer*, 1993. [Online]. Available: http://www.springer.com/gp/book/9780792324928. [Accessed: 25-Feb-2016].

[30] G. R. Cowper, "The Shear Coefficient in Timoshenko's Beam Theory," *J. Appl. Mech.*, vol. 33, no. 2, pp. 335–340, Jun. 1966.